Asian Journal of Chemistry; Vol. 34, No. 5 (2022), 1279-1283

ASIAN JOURNAL OF CHEMISTRY

https://doi.org/10.14233/ajchem.2022.23606

Optical and Magnetic Characteristics of $LaFeO_3$ Nanoparticles Synthesized by Simple Co-Precipitation Method using Ethanol

PHAM THI HONG DUYEN[1], NGUYEN ANH TIEN[2] and BUI XUAN VUONG[3,*]

[1]Institute of Applied Technology, Thu Dau Mot University, Thu Dau Mot City, Binh Duong Province 590000, Vietnam
[2]Faculty of Chemistry, Ho Chi Minh City University of Education, Ho Chi Minh City 700000, Vietnam
[3]Faculty of Pedagogy in Natural Sciences, Sai Gon University, Ho Chi Minh City 700000, Vietnam

*Corresponding author: E-mail: buixuanvuongsgu@gmail.com

Received: 3 November 2021; *Accepted*: 7 March 2022; *Published online*: 20 April 2022; AJC-20783

Present study describes the synthesis of nanocrystalline lanthanum orthoferrite by co-precipitation method using ethanol as a solvent. $LaFeO_3$ nanopowders formed after annealing the precursor at temperatures of 700, 800 and 900 ºC for 1 h, have a particle size in the range of 30-50 nm. According to XRD analysis, an increase in the annealing temperature from 700 to 900 ºC leads to an increase in the average crystallite size from 43.76 to 62.80 nm and a decrease in the unit cell volume of about 241.90 to 240.66 $Å^3$. Synthesized $LaFeO_3$ nanoparticles have strong absorption in ultraviolet (~ 200-400 nm) and visible light (~ 400-600 nm) and are soft magnetic materials with high magnetization.

Keywords: Nanocrystals, Lanthanum orthoferrite, Ethanol, Optical properties, Magnetic properties, Co-precipitation method.

INTRODUCTION

$LaFeO_3$ with a perovskite structure is one of the important orthoferrites of rare earth elements due to a wide range of properties important for application, especially electrical, optical and magnetic properties with high sensitivity to particle size reduction to nanometer values [1-6]. The properties of orthoferrite rare earth materials depend not only on the particle size and morphology, but also on the content of the dopant and the method of preparation [4,7-10].

Now, for the synthesis of nanocrystalline orthoferrites of lanthanide elements $LnFeO_3$ (Ln = La, Y, Ho, Nd, Pr, Tm, Lu, *etc*.) a wide variety of techniques have been developed, for example, mechanochemical [11,12], hydrothermal synthesis [13], co-precipitation method [4,14,15], sol-gel technology [16-20], *etc*. A special place is occupied by the sol-gel method, which allows obtaining nanopowders with a narrow particle size distribution at relatively low annealing temperatures. The process of synthesis of orthoferrites by the sol-gel method requires compliance with a number of factors affecting the formation of single-phase products, for example, temperature and time of annealing, temperature and time of gel formation, pH value of the medium, molar ratio of the gel-forming substance and cations . The main problem is associated with the choice of the organic polymer used for gel formation, which leads to significant time costs. Earlier, we synthesized nanocrystalline orthoferrite $HoFeO_3$ with an average crystal size of the order of < 50 nm by a simple co-precipitation method *via* hydrolysis of Ho(III) and Fe(III) cations in hot ethanol (T = ~ 78 ºC) followed by the addition of a 5% NH_3 solution [21]. Ethanol was chosen as a solvent due to the lower dipole moment of the ethanol molecule compared to the dipole moment of water [$\mu(C_2H_5OH)$ = 1.66 D, $\mu(H_2O)$ = 1.85 D] [22,23]. At the same time, the viscosity of C_2H_5OH (1.2 10^{-3} Pa·s) is significantly lower than that of organic polymers used for the synthesis of nanoparticles by the sol-gel method [23]. Consequently, the cations of the rare-earth elements Ln(III) and Fe(III) inter-act worse in the presence of C_2H_5OH, which leads to a decrease in the particle size of the $LnFeO_3$ orthoferrite. In the case of using water as a solvent, a side hydroxo-complexation process is possible due to the cations Ln(III) and Fe(III), which makes the synthesis of nanocrystals less controllable than in an ethanolic medium.

The aim of this study was the synthesis and investigation of the structural, optical and magnetic characteristics of nanocrystalline lanthanum orthoferrite formed by co-precipitation method using ethanol as solvent.

EXPERIMENTAL

The following reagents were used as starting materials *viz*. $La(NO_3)_3{\cdot}6H_2O$ (99.8%, Merck), $Fe(NO_3)_3{\cdot}9H_2O$ (99.6%, Sigma-Aldrich), absolute ethanol (99.7%, D = 0.79 g mL^{-1}), ammonia solution (Xilong, 85%, D = 0.91 g mL^{-1}), distilled water and phenolphthalein test paper.

The procedure for the synthesis of lanthanum orthoferrite nanopowders is based on a similar method that reported earlier [21]. To 400 mL of boiling ethanol (~ 78 ºC), 50 mL of an equimolar mixture of 0.1 M of $La(NO_3)_3$ and 0.1 M of $Fe(NO_3)_3$ were added using magnetic stirrer. The resulting sol was boiled for another 10 min and then cooled to room temperature (~ 300 K). The sol acquired a yellow-brown colour. A 5% NH_3 solution was added dropwise to it while stirring with a magnetic stirrer. The ammonia solution was used as a precipitant in the amount required for the complete precipitation of La^{3+} and Fe^{3+} cations (tested with phenolphthalein test paper). The precipitate was stirred for 60 min with a magnetic stirrer. After separation on a vacuum filter, it was washed with distilled water until a pH of ~ 7 was reached (determined using lithmus paper), dried at room temperature to constant weight (for about 3-5 days) and grounded. The resulting yellow-brown powder served as a precursor for the preparation of $LaFeO_3$ orthoferrite.

Thermogravimetry (TGA) and differential scanning calorimetry (DSC) were performed using dry air at a heating rate of 10 K min^{-1} and a maximum temperature of 900 ºC in platinum crucibles with a Labsys Evo-TG-DSC 1600 ºC synchronous thermal analyzer (France). X-ray diffraction analysis (XRD) of synthesized $LaFeO_3$ samples was carried out using an D8-ADVANCE X-ray diffractometer (Germany) (Cu*K*α radiation, λ = 1.5406 Å, angle range 2θ = 20-70º, scanning step 0.019 º/s). The crystal size (D_{XRD}, nm) of $LaFeO_3$ samples was determined using the Scherrer equation, the parameters of the crystal lattice (*a*, *b*, *c*, *V*) were calculated by the method as described earlier [24,25].

The quantitative composition and distribution of chemical elements (La, Fe, O) over the sample surface were investigated by energy dispersive X-ray spectroscopy (EDX) using an FE-SEM S-4800 scanning electron microscope (Japan). The quantitative elemental composition was determined as the average for the values obtained at five different points of each sample. Crystal size and morphology of the obtained $LaFeO_3$ samples were determined by scanning electron microscopy (SEM, S-4800, Japan) and transmission electron microscopy (TEM, Joel JEM-1400, Japan). The absorption spectra of $LaFeO_3$ nanocrystals were recorded using a UV-visible spectrophotometer (UV-Vis, JASCO V-550, Japan). The optical energy gap (bandgap) was calculated by the as method described earlier [26].

Hysteresis loop and magnetic properties, including coercive force (H_c, Oe), remanent magnetization (M_r, emu g^{-1}) and saturation magnetization (M_s, emu g^{-1}) were recorded using a MICRO-SENE EV11 magnetometer with a vibrating sample under the action of a magnetic field in the range from -21,000 Oe to +21,000 Oe.

RESULTS AND DISCUSSION

The TGA and DSC curves obtained for the precursors of nanocrystalline lanthanum orthoferrite (*o*-$LaFeO_3$) are shown in Fig. 1. The total mass loss at temperatures from 50 ºC to 900 ºC was 30.7%. This indicates the formation of bonds between La(III) and Fe(III) cations with C_2H_5-groups in the sediment [21]. Indeed, if the precipitate would contain only iron(III) and lanthanum hydroxides, the mass loss calculated using the eqn. 1 would be 18.2%.

$$La(OH)_3 + Fe(OH)_3 \longrightarrow LaFeO_3 + 3H_2O \quad (1)$$

$$\Delta m_{loss} = \frac{3.18}{189.91+106.85} \times 100\% = 18.2\%$$

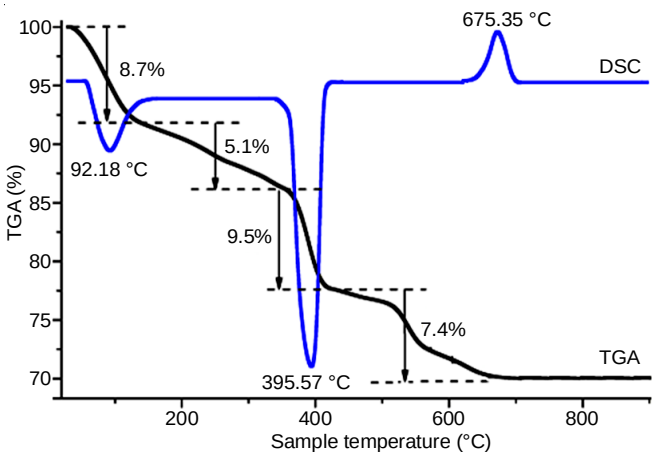

Fig. 1. TGA and DSC curves for dried powders synthesized by co-precipitation method using ethanol

The mass loss caused by the destruction of M^{3+}–C_2H_5 bonds (M = La, Fe), dehydration and decomposition of lanthanum and iron(III) hydroxides, corresponds to endothermic peaks at 92.56 and 395.57 ºC on the DSC curve (Fig. 1). Similar results were obtained in earlier studies for $HoFeO_3$ and $PrFeO_3$ orthoferrites [21,27]. The exothermic peak at 675.35 ºC corresponds to the phase formation of $LaFeO_3$ orthoferrite from La_2O_3 and Fe_2O_3 in accordance with the eqn. 2:

$$La_2O_3 + Fe_2O_3 \longrightarrow 2LaFeO_3 \quad (2)$$

This conclusion is in good agreement with the change in mass on the TGA curve, when no noticeable changes in the sample mass were observed at temperatures above ~ 700 ºC.

Based on the results of thermal analysis, the precursors were annealed at temperatures of 700, 800, and 900 ºC for an hour at a heating rate of 10 deg min^{-1}. It follows from the XRD data that all the synthesized samples are a single-phase product with the structure of lanthanum orthoferrite (card no. 01-070-7777) (Figs. 2 and 3) and all identified peaks correspond to standard *o*-$LaFeO_3$ peaks.

The crystallinity of $LaFeO_3$ samples increased as expected as the annealing temperature increased, as was evidenced by the narrowing (area reduction) of the noise reduction peaks.

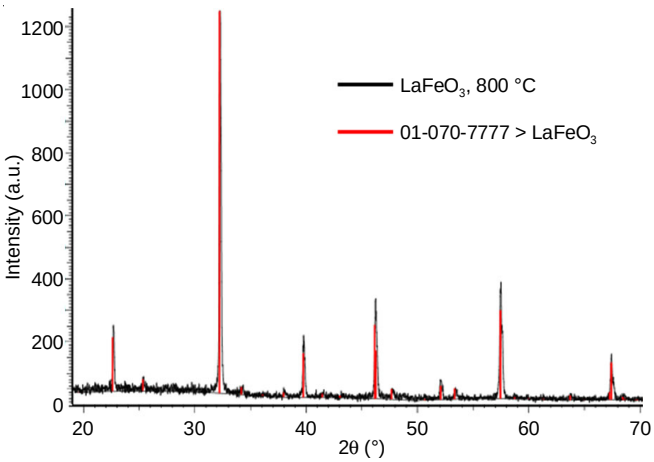

Fig. 2. XRD pattern of $LaFeO_3$ nanopowders annealed at 800 °C for 1 h

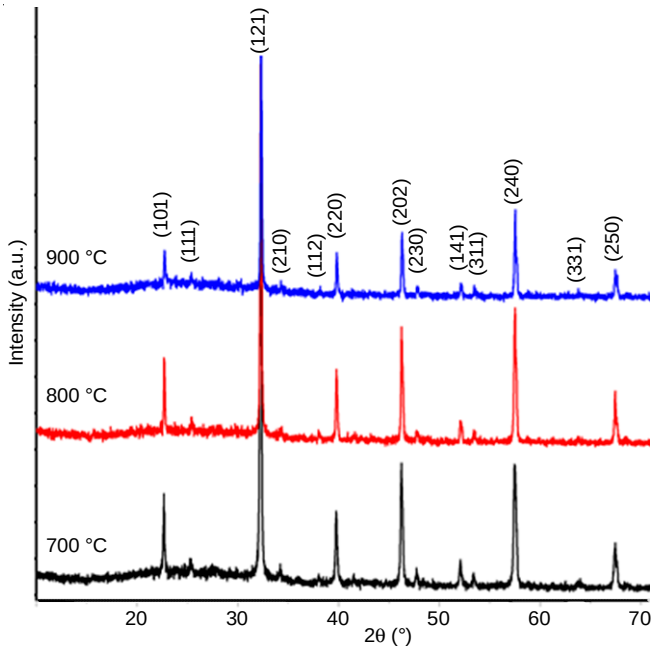

Fig. 3. XRD patterns of $LaFeO_3$ nanopowders annealed at 700, 800 and 900 °C for 1 h

Determination of the average diameter (D_{av}, nm) of nanopowder crystals and unit cell parameters (calculation based on XRD data) showed that an increase in the annealing temperature leads to an increase in D_{av} from 43.76 to 62.80 nm and a decrease in cell volume from 241.90 to 240.66 $Å^3$ (Table-1).

TABLE-1
AVERAGE CRYSTAL SIZE AND UNIT CELL PARAMETERS OF $LaFeO_3$ NANOPOWDERS ANNEALED AT 700, 800, AND 900 °C FOR 1 h

	700 °C	800 °C	900 °C
D, nm	43.76	47.25	62.80
a (Å)	5.574	5.566	5.562
b (Å)	7.845	7.832	7.833
c (Å)	5.532	5.536	5.524
V, $Å^3$	241.90	241.33	240.66

Morphology: The SEM and TEM images of $LaFeO_3$ nano-powders after annealing at 800 ºC for an hour are shown in Fig. 4. The synthesized $LaFeO_3$ nanoparticles were isometric and their size was 30-50 nm. The average particle size determined by TEM was 45.33 ± 3.17 nm.

Analysis of the EDX pattern of an $LaFeO_3$ sample, annealed at 800 ºC, showed that the peaks correspond to only three elements: La, Fe, and O (Fig. 5). Table-2 shows the average values of the mass fractions and atomic percentages of La, Fe, and O, obtained based on measurements at five different regions of the sample. These results are consistent with the proposed chemical composition (Table-2). The product yield (m_{exp}/ m_{cal}) was from 96 to 98%.

UV-visible studies: The UV-visible absorption spectra of $LaFeO_3$ nanopowders after annealing at various temper-

TABLE-2
EDX ANALYSIS OF $LaFeO_3$ NANOPOWDERS ANNEALED AT 800 °C FOR 1 h

La		Fe		O	
mass. %	at. %	mass. %	at. %	mass. %	at. %
56.17	18.22	20.74	16.73	23.09	66.04

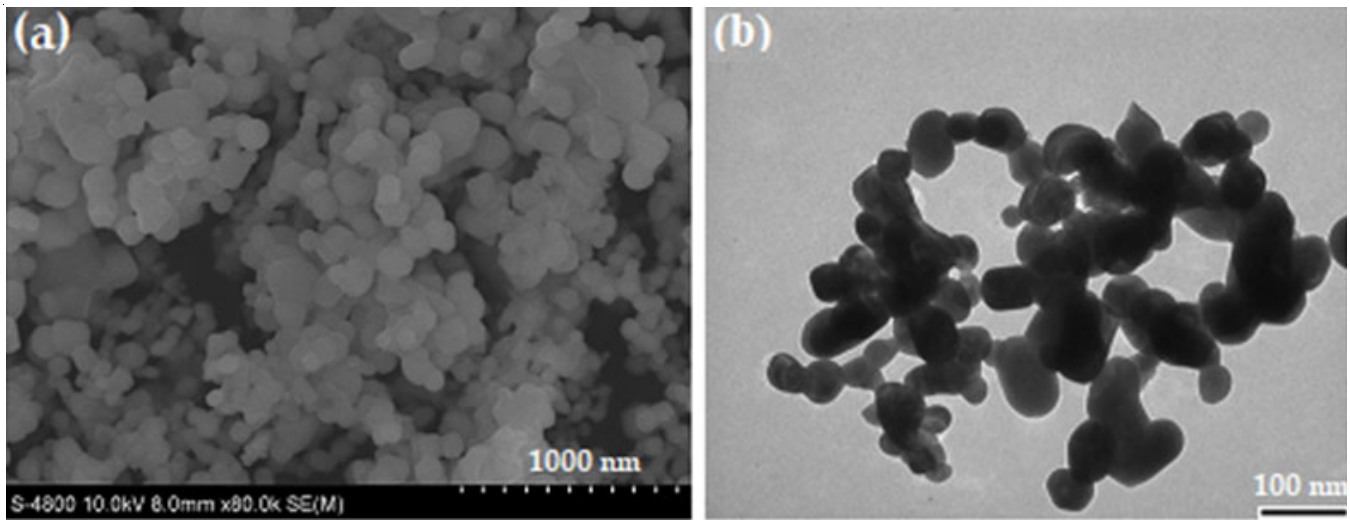

Fig. 4. (a) SEM and (b) TEM images of an $LaFeO_3$ sample annealed at 800 °C for 1 h

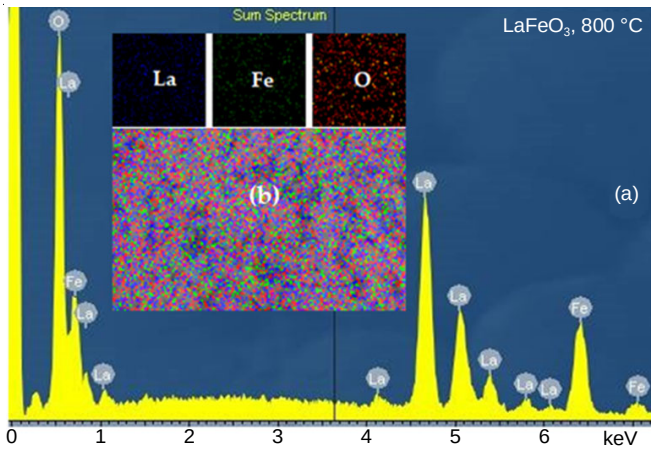

Fig. 5. EDX spectrum (a) and EDX-mapping (b) of $LaFeO_3$ sample annealed at 800 °C for 1 h

atures for an hour are shown in Fig. 6. All synthesized samples showed strong absorption in ultraviolet (~ 200-400 nm) and visible light (~ 400-600 nm) (Fig. 6a). Therefore, the synthesized $LaFeO_3$ nanopowders can be used as new catalysts in visible light [4,12,16,20]. The optical energy gap (bandgap) for all $LaFeO_3$ samples were 2.16-2.01 eV (Fig. 6b) and close to the values determined for $LaFeO_3$ in other studies [4,20].

Magnetic studies: Dependence of the magnetization of $LaFeO_3$ nanocrystals on the magnetic field strength at a temperature of 300 K is shown in Fig. 7. Coercive force (H_c = 82.2–108.3 Oe) and the remanent magnetization ($M_r = 4.9 \times 10^{-3}$–15.6×10^{-3} emu g^{-1}) of all three studied $LaFeO_3$ samples was significantly lower than that of $LaFeO_3$ synthesized by the co-precipitation method from the aqueous solutions described by Sasikala *et al.* [4] (H_c = 1217.6 Oe, $M_r = 542.9 \times 10^{-3}$ emu g^{-1}) however, were closed to the $LaFeO_3$ sample obtained by the sol-gel method using citric acid and ethylene glycol reported by Phoka *et al.* [20] (H_c = 75-125 Oe) (Table-3). However, the synthesized $LaFeO_3$ crystallites were characterized by a higher value of magnetization compared to $LaFeO_3$ nanoparticles as

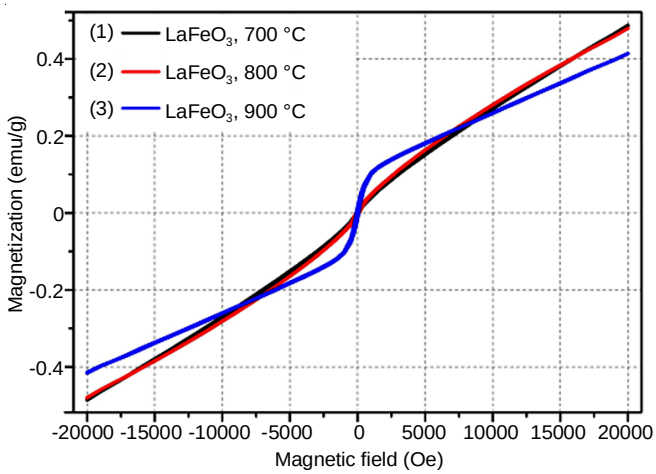

Fig. 7. Field dependence of the magnetization of $LaFeO_3$ nanocrystals annealed at 700, 800 and 900 °C for 1 h

TABLE-3
OPTICAL AND MAGNETIC CHARACTERISTICS OF $LaFeO_3$ NANOPOWDERS ANNEALED AT 700, 800 AND 900 °C FOR 1 h

Samples	H_c (Oe)	M_r (emu g^{-1})	M_s (emu g^{-1})	E (eV)
$LaFeO_3$, 700 °C	82.2	4.9×10^{-3}	0.48	2.16
$LaFeO_3$, 800 °C	108.3	6.8×10^{-3}	0.49	2.10
$LaFeO_3$, 900 °C	89.3	15.6×10^{-3}	0.42	2.01
$LaFeO_3$ [4]	1217.6	542.9×10^{-3}	0.0065	2.05
$LaFeO_3$ [20]	25-125	–	0.10-0.09	2.15-2.23

reported by other researchers [4,20] (Table-3). None of the tested $LaFeO_3$ samples reach magnetic saturation in a magnetic field of 21000 Oe (Fig. 7), which indicates the ability of such materials to operate in a high magnetic field.

Conclusion

The $LaFeO_3$ nanocrystals were formed by co-precipitation method in ethanolic medium with subsequent annealing at various temperatures (700, 800 and 900 °C) for 1 h. With an increase in the annealing temperature from 700 to 900 ºC, the

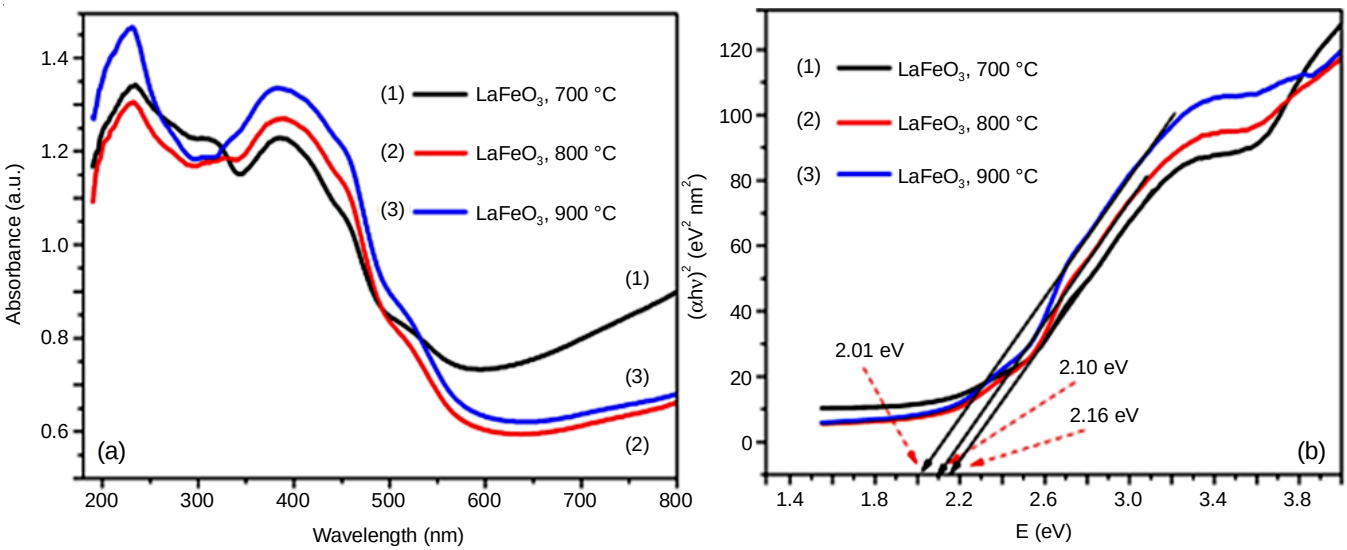

Fig. 6. UV-vis absorption spectra (a) and plot of $(Ahν)^2$ as a function of photon energy (b) for $LaFeO_3$ nanoparticles annealed at 700, 800 and 900 °C for 1 h

average crystallite size increased from 43.76 to 62.80 nm, the unit cell volume decreased from 241.90 to 240.66 $Å^3$ and the energy gap decreased from 2.16 to 2.01 eV. The UV-Vis spectra showed that the synthesized $LaFeO_3$ nanoparticles have strong absorption in the UV-visible light. The resulting $LaFeO_3$ nanopowders are a soft magnetic material with low coercive force and remanent magnetization and high saturation magnetization.

CONFLICT OF INTEREST

The authors declare that there is no conflict of interests regarding the publication of this article.

REFERENCES

1. U. Oemar, P. Ang, K. Hidajat and S. Kawi, *Int. J. Hydrogen Energy*, **38**, 5525 (2013); https://doi.org/10.1016/j.ijhydene.2013.02.083
2. J.W. Fergus, *Sens. Actuators B Chem.*, **123**, 1169 (2007); https://doi.org/10.1016/j.snb.2006.10.051
3. M.V. Knurova, I.Ya. Mittova, N.S. Perov, O.V. Al'myasheva, N.A. Tien, V.O. Mittova, V.V. Bessalova and E.L. Viryutina, *Russ. J. Inorg. Chem.*, **62**, 281 (2017); https://doi.org/10.1134/S0036023617030081
4. C. Sasikala, N. Durairaj, I. Baskaran, B. Sathyaseelan, M. Henini and E. Manikandan, *J. Alloys Compd.*, **712**, 870 (2017); https://doi.org/10.1016/j.jallcom.2017.04.133
5. A.T. Nguyen, V.N.T. Pham, H.T. Le, D.H. Chau, V.O. Mittova, L.T.T. Nguyen, D.A. Dinh, T.V. Nhan Hao and I.Y. Mittova, *Ceram. Int.*, **45**, 21768 (2019); https://doi.org/10.1016/j.ceramint.2019.07.178
6. N.F. Atta, A. Galal and E.H. El-Ads, Eds.: L. Pan and G. Zhu, Perovskite Nanomaterials: Synthesis, Characterization and Applications, InTechOpen: London, Ed.: 1, Chap. 4, pp. 107-151 (2016)
7. L. Zhang, X. Zhang, G. Tian, Q. Zhang, M. Knapp, H. Ehrenberg, G. Chen, Z. Shen, G. Yang, L. Gu and F. Du, *Nat. Commun.*, **11**, 3490 (2020); https://doi.org/10.1038/s41467-020-17233-1
8. N.A. Tien, I.Y. Mittova, D.O. Solodukhin, O.V. Al'myasheva, V.O. Mittova and S.Y. Demidova, *Russ. J. Inorg. Chem.*, **59**, 40 (2014); https://doi.org/10.1134/S0036023614020156
9. M.V. Berezhnaya, O.V. Al'myasheva, V.O. Mittova, A.T. Nguen and I.Y. Mittova, *Russ. J. Gen. Chem.*, **88**, 626 (2018); https://doi.org/10.1134/S1070363218040035
10. V.I. Popkov, E.A. Tugova, A.K. Bachina and O.V. Almyasheva, *Russ. J. Gen. Chem.*, **87**, 2516 (2017); https://doi.org/10.1134/S1070363217110020
11. V. Berbenni, G. Bruni, C. Milanese, A. Girella and A. Marini, *J. Therm. Anal. Calorim.*, **133**, 413 (2018); https://doi.org/10.1007/s10973-017-6878-z
12. ZhQ. Wang, Y.Sh. Lan, Z.-Y. Zeng, X.-R. Chen and Q.-F. Chen, *Solid State Commun.*, **288**, 10 (2019); https://doi.org/10.1016/j.ssc.2018.11.004
13. Zh. Zhou, L. Guo, H. Yang, Q. Liu and F. Ye, *J. Alloys Comp.*, **583**, 21 (2014); https://doi.org/10.1016/j.jallcom.2013.08.129
14. A.T. Nguyen, V. Pham, T.L. Pham, L.T.T. Nguyen, I.Y. Mittova, V.O. Mittova, L.N. Vo, B.T.T. Nguyen, V.X. Bui and E.L. Viryutina, *Crystals*, **10**, 219 (2020); https://doi.org/10.3390/cryst10030219
15. A.T. Nguyen, V. Pham, T.T.L. Nguyen, V.O. Mittova, Q.M. Vo, M.V. Berezhnaya, I.Y. Mittova, T.H. Do and H.D. Chau, *Solid State Sci.*, **96**, 105922 (2019); https://doi.org/10.1016/j.solidstatesciences.2019.06.011
16. S.N. Tijare, M.V. Joshi, P.S. Padole, P.A. Mangrulkar, S.S. Rayalu and N.K. Labhsetwar, *Int. J. Hydrogen Energy*, **37**, 10451 (2012); https://doi.org/10.1016/j.ijhydene.2012.01.120
17. T. Liu and Y. Xu, *Mater. Chem. Phys.*, **129**, 1047 (2011); https://doi.org/10.1016/j.matchemphys.2011.05.054
18. K. Parida, K.H. Reddy, S. Martha, D.P. Das and N. Biswal, *Int. J. Hydrogen Energy*, **35**, 12161 (2010); https://doi.org/10.1016/j.ijhydene.2010.08.029
19. M. Popa, J. Frantti and M. Kakihana, *Solid State Ion.*, **154-155**, 437 (2002); https://doi.org/10.1016/S0167-2738(02)00480-0
20. S. Phokha, S. Pinitsoontorn, S. Maensiri and S. Rujirawat, *J. Sol-Gel Sci. Technol.*, **71**, 333 (2014); https://doi.org/10.1007/s10971-014-3383-8
21. A.T. Nguyen, T.T.L. Nguyen, V.X. Bui, D.H.T. Nguyen, H.D. Lieu, L.M.T. Le and V. Pham, *J. Alloys Compd.*, **834**, 155098 (2020); https://doi.org/10.1016/j.jallcom.2020.155098
22. C.E. Housecroft and A.G. Sharpe, Inorganic Chemistry, Pearson: Prentice Hall, Ed.: 2 (2005).
23. D. Klein, Organic Chemistry, Wiley, Ed.: 2, Chap. 13 (2016).
24. M. Abdellahi, A.S. Abhari and M. Bahmanpour, *Ceram. Int.*, **42**, 4637 (2016); https://doi.org/10.1016/j.ceramint.2015.12.027
25. A.T. Nguyen, N.T. Nguyen, I. Mittova, N. Perov, V. Mittova, T. Hoang, V. Nguyen, V. Nguyen, V. Pham and X. Bui, *Process. Appl. Ceram.*, **14**, 355 (2020); https://doi.org/10.2298/PAC2004355N
26. N. Ghobadi, *Int. Nano Lett.*, **3**, 2 (2013); https://doi.org/10.1186/2228-5326-3-2
27. X.V. Bui and A.T. Nguyen, *Conden. Matt. Interphases*, **23**, 196 (2021); https://doi.org/10.17308/kcmf.2021.23/3429